

# TelemetRing: A Batteryless and Wireless Ring-Shaped Keyboard using Passive Inductive Telemetry

Ryo Takahashi<sup>1</sup>, Masaaki Fukumoto<sup>2</sup>, Changyo Han<sup>1</sup>,  
Takuya Sasatani<sup>1</sup>, Yoshiaki Narusue<sup>1</sup>, Yoshihiro Kawahara<sup>1</sup>

<sup>1</sup>The University of Tokyo <sup>2</sup>Microsoft Corporation  
 {takahashi, sasatani, kawahara}@akg.t.u-tokyo.ac.jp fukumoto@microsoft.com  
 hanc@nae-lab.org narusue@mlab.t.u-tokyo.ac.jp

## ABSTRACT

TelemetRing is a batteryless and wireless ring-shaped keyboard that supports command and text entry in daily lives by detecting finger typing on various surfaces. The proposed inductive telemetry approach eliminates bulky batteries or capacitors from the ring part. Each ring consists of a sensor coil (the ring part itself), 1-DoF piezoelectric accelerometer, and varactor diode; moreover, it has different resonant frequencies. Typing shocks slightly shift the resonant frequency, and these are detected by a wrist-mounted readout coil. 5-bit chord keyboard is realized by attaching five sensor rings on five fingers. Our evaluation shows that the prototype achieved the tiny (6 g, 3.5 cm<sup>3</sup>) ring sensor and 89.7% of typing detection ratio.

## Author Keywords

Batteryless; keyboard; ring; coil; wearable; wireless.

## CCS Concepts

•Human-centered computing → Keyboards;

## INTRODUCTION

As wearable devices (*e.g.*, smartglasses and smartwatches) are being tightly interwoven into our daily lives, an easy-to-carry and always-available input device is desirable to interact with these devices [22, 10, 35]. A wireless ring-shaped keyboard, which supports text entry by detecting finger typing, is one of the promising approaches [11, 23]. This approach supports text input anytime and anywhere, since (a) the keyboard function is implemented within the form-factor of rings and wristbands, both of which are already widely accepted as accessories and (b) can be used on everyday surfaces (*e.g.*, desk and knee).

However, previous wireless ring-shaped keyboards required batteries attached to each ring device to empower the active

Permission to make digital or hard copies of all or part of this work for personal or classroom use is granted without fee provided that copies are not made or distributed for profit or commercial advantage and that copies bear this notice and the full citation on the first page. Copyrights for components of this work owned by others than ACM must be honored. Abstracting with credit is permitted. To copy otherwise, or republish, to post on servers or to redistribute to lists, requires prior specific permission and/or a fee. Request permissions from [Permissions.acm.org](http://Permissions.acm.org).

UIST '20, October 20–23, 2020, Virtual Event, USA

ACM 978-1-4503-7514-6/20/10...\$15.00

DOI: <http://dx.doi.org/10.1145/3379337.3415873>

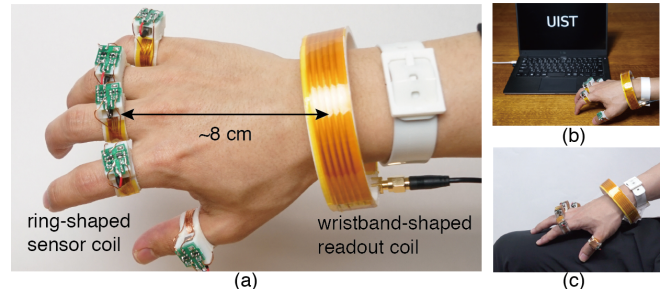


Figure 1. (a) Overview of TelemetRing. TelemetRing supports text entry by typing on various surfaces such as (b) hard desk and (c) soft knee.

components (*e.g.*, microcontrollers and wireless communication modules) [5, 11, 23]. The bulky batteries on the ring devices make them uncomfortable to wear and necessitate the users to charge them periodically. To overcome these challenges, we propose a batteryless and wireless ring-shaped keyboard named TelemetRing.

## RELATED WORK

### Wearable Keyboards

*Wearable keyboards* [10], which enable text input anytime and anywhere without distracting from daily activities, can be categorized into two types: hand gesture-based methods (*e.g.*, hand waving, handwriting, fist, and pinch) and finger typing-based methods (*i.e.*, single or multiple finger typing).

As for the hand gesture-based methods, many studies leverage computer vision [8, 19, 34]. However, these approaches require the hands to be in line-of-sight with the camera. Therefore, various sensor-based approaches for detecting hand gestures have been explored as follows: inductive tracking [9, 15, 16, 28, ?], touch sensing using the body as an electric waveguide [36], electromyography (EMG) [32, 33], bio-acoustic sensing [14, 18], and inertial measurement of users' hand [13, 21]. However, these approaches can not detect subtle text-input action such as finger typing; therefore, long and exaggerated gestures, which cause fatigue and slow down input speed [12], are required.

Meanwhile, finger typing enables high-speed text typing, requires small force, and can be used on various surfaces. Furthermore, prior work proposed wireless ring-shaped keyboards,

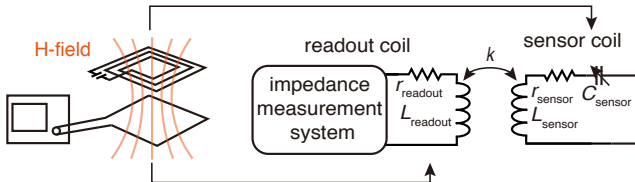


**Figure 2.** Conventional passive inductive telemetry. It consists of a readout coil connected to an impedance measurement system (*e.g.*, a vector network analyzer) and a sensor coil that passively changes its impedance based on the sensing target.

for finger typing without being disturbed by wires. These consist of i) five rings equipped with shock sensors that can detect subtle shock waves caused by typing motions and ii) a wristband equipped with a readout circuit. The output of the shock sensors is sent to the wristband based on wireless communication methods such as Wi-Fi [23], body channel communication [11], or WISP [5] to detect typing. However, batteries are necessary for each ring to drive the active components (*e.g.*, communication modules); this makes the ring bulky and requires periodic charging.

#### Wireless Power Transfer

Wireless power transfer from a battery-equipped wristband transmitter to the batteryless rings seems to be a promising approach towards achieving a batteryless and wireless ring-shaped keyboard; it is known that, by leveraging resonant coils, power can be sent between mid-range distances [20]. However, our preliminary measurements indicated that the available power transfer efficiency between a 9.0 cm diameter wristband-shaped transmitter coil and a 1.8 cm diameter ring-shaped receiver coil with a distance of 8 cm is below 1% at the operating frequency of 6.78 MHz. This is because the inductive coupling coefficient between these coils significantly reduces ( $k : 0.005 \sim 0.006$ ) owing to the size difference and the long distance between the coils [31]. Since the output power is restricted by the ICNIRP guidelines [26] and the power capacity of the wristband is limited, low power transfer efficiency (1%) makes this approach non-practical.

#### PASSIVE INDUCTIVE TELEMETRY

To achieve batteryless ring-shaped sensors, we leverage a wireless sensing technology termed passive inductive telemetry, as shown in Fig. 2. This approach uses a sensor coil and a readout coil, both of which are inductively coupled to each other [6, 27, 15]. As the impedance variation of the sensor coil affects the input impedance of the coupled readout coil, the sensor value can be read out wirelessly by connecting the readout coil to an impedance measurement system (*e.g.*, a vector network analyzer). In particular, this impedance change is most clearly observed near the resonant frequency of the sensor coil. One of the greatest advantages of the passive inductive telemetry is that the telemetry does not require the sensor coil to be equipped with the batteries, which enables us to design batteryless ring-shaped sensors.

However, there are two key challenges for enabling batteryless ring sensors using passive inductive telemetry. First, we con-

firmed that the inductive coupling is very weak ( $k : 0.005 \sim 0.006$ ) when these devices are designed to fit around our wrists and fingers (ring-shaped sensor coils with a diameter of 1.5 cm~1.8 cm and a wristband-shaped readout coil with a diameter of 9 cm, placed 8 cm apart). Owing to this weak coupling, the impedance change observed from the readout coil becomes extremely small. Unfortunately, conventional inductive telemetry cannot be applied since it requires a relatively strong inductive coupling ( $k : \sim 0.1$ ) [17]. Second, for multiple fingers' input, our readout coil needs to simultaneously read out multiple sensor coils with low latency, since the shock wave period by typing is so short (< 5 ms) [10]. Therefore, we must implement highly-sensitive inductive telemetry in a frequency-division multiplexing (FDM) form.

#### CONTRIBUTION

To achieve FDM links between the rings and the wristband, we develop a novel passive inductive telemetry system. As will be discussed later, our telemetry employs the following two key technologies: distributed reactance compensation (DRC) and a balanced bridge circuit. DRC enables us to read out the small impedance changes even under weak coupling conditions, whereas the balanced bridge circuit can construct five highly-sensitive inductive channels at different frequencies. Taken together, we can simultaneously achieve the detection of typing and classification of the typed finger. To examine the feasibility of our design, we built a prototype shown in Fig. 1, and evaluated the typing recognition rate with it.

#### SYSTEM DESIGN

As shown in Fig. 3 (a), our system is composed of three types of components: 1) five ring-shaped sensor coils that change their impedance through typing, 2) a wristband-shaped readout coil that is inductively coupled with five rings, and 3) an impedance measurement system comprising a software defined radio (SDR) and a balanced bridge circuit. In brief, our system performs the following steps: First, the shock wave caused by the typing changes the impedance of the ring worn on the typed finger. Next, the impedance change of each ring induces a small impedance change in the wristband via inductive coupling. Finally, the impedance measurement system detects this small impedance change on the wristband and distinguishes the typing fingers through our signal processing.

#### Ring-shaped Sensor Coil

To realize ring-shaped sensor coils that passively change its impedance by typing, we design a shock-sensitive variable capacitor by combining a piezoelectric accelerometer (*i.e.*, piezo) and varactor diodes (*i.e.*, varactor). Owing to the piezoelectric effect, the piezo element generates an voltage by the typing shock, and this reverse bias voltage is applied to the varactors, which results in changing the capacitance of the varactor. Additional parallel capacitors are connected to the varactors to set the resonant frequency of the default state (*i.e.*, when no shock is applied). Since each of these five rings has a different resonant frequency, the readout coil enables to distinguish the response from each sensor coil.

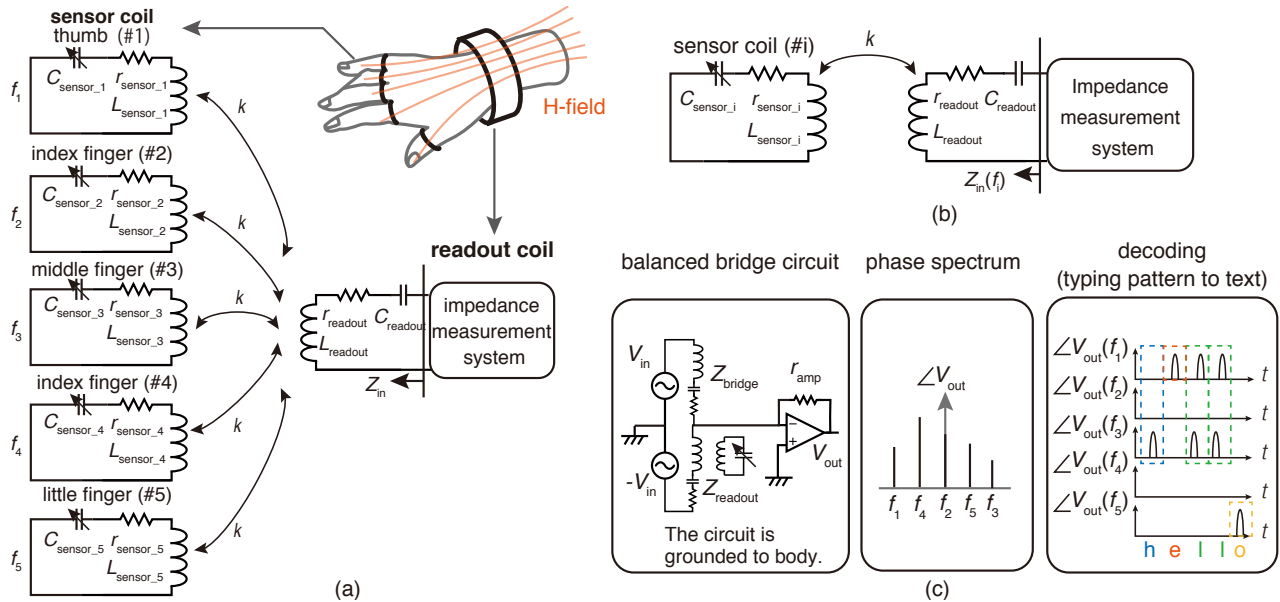


Figure 3. (a) System overview of TelemetRing. It consists of 1) five ring-shaped sensor coils, 2) a wristband-shaped readout coil, and 3) an impedance measurement system. (b) Equivalent circuit model at the resonant frequency of sensor coil #i. (c) Overview of our impedance measurement system.

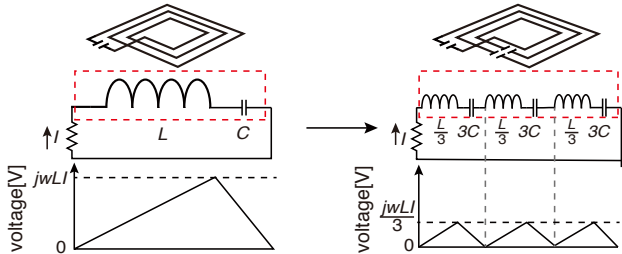


Figure 4. Overview of distributed reactance compensation (DRC). DRC mitigates the effects occurring owing to wavelength and suppresses the electric energy from the capacitor by inserting multiple series capacitors into the coil.

### Distributed Reactance Compensation

Next, we explain how to increase the impedance change at the readout coil, even under weak inductive coupling conditions. To better understand this challenge, we first explain how each sensor coil affects the impedance of the readout coil. Since each sensor coil has different resonant frequencies (\$f\_i : i = 1, \dots, 5\$), and each ring significantly affects the readout coil only when operated at the resonant frequency of itself, the other four sensor coils off-resonance can be neglected. Note that \$f\_1 \dots f\_5\$ are assigned to five sensor coils as follows (\$f\_1\$: 12.16 MHz, \$f\_2\$: 13.46 MHz, \$f\_3\$: 14.46 MHz, \$f\_4\$: 12.76 MHz, and \$f\_5\$: 13.96 MHz). Therefore, the circuit model can be simplified, as shown in Fig. 3 (b) when operated at the resonant frequency of the \$i\$-th sensor coil, \$f\_i\$. Thus, at angular frequency \$\omega\_i (= 2\pi f\_i)\$, the input impedance of our readout coil, \$Z\_{\text{in}}(f\_i)\$, can be expressed as follows:

$$Z_{\text{in}}(f_i) \doteq Z_{\text{readout}} + \frac{(\omega_i M)^2}{Z_{\text{sensor}_i}} \quad (1)$$

where \$M (= k \sqrt{L\_{\text{readout}} L\_{\text{sensor}\_i}}\$, \$k : 0.005 \sim 0.006\$) is the mutual inductance between the readout coil and the sensor coil

#i. Based on Eq. (1), the change of \$Z\_{\text{in}}(f\_i)\$, induced by the change of \$Z\_{\text{sensor}\_i}\$ can be expressed as follows:

$$\Delta Z_{\text{in}}(f_i) \doteq \Delta \left\{ \frac{(\omega_i M)^2}{Z_{\text{sensor}_i}} \right\} \quad (2)$$

Eq. (2) shows that this variation can be enlarged by increasing \$\omega M\$. However, the weak inductive coupling (\$k : 0.005 \sim 0.006\$) makes \$M\$ small, and thus, \$\Delta Z\_{\text{in}}(f\_i)\$ is hard to observe. While it can be solved by increasing \$L\_{\text{readout}}\$ and \$L\_{\text{sensor}}\$, the inductance is limited because the short-wavelength restricts the number of turns at higher frequencies.

To address this issue, we employ DRC [25, 24] for both the readout coil and the five sensor coils. As shown in Fig. 4, DRC mitigates the effects occurring owing to wavelength (stray capacitor etc.) by inserting multiple series capacitors into the coil; this enables a larger number of turns and consequently, a higher inductance. Furthermore, the voltage applied to multiple capacitors becomes \$1/N\$ (\$N\$: the number of capacitor) for the input current \$I\$, and thus, the electric loss of each capacitor becomes \$1/N^2\$ [25]; this means that DRC can mitigate the electric field interference between the coil and the dielectric human hand, even at the high frequency. So far, DRC has been used in the field of wireless power transfer (WPT) to build large transmitter coils, which were not available owing to the effect of wavelength [24]. In contrast, TelemetRing applies DRC to i) increase the inductance of the sensor coils and the readout coil and ii) suppress the electric field interference with the human hand.

### Impedance Measurement System

Finally, we proceed to the impedance measurement system. To measure such a small impedance change, and moreover, distinguish the typed finger, TelemetRing employs an impedance measurement system consisting of an SDR and a balanced bridge circuit, as shown in Fig. 3(c). The SDR emits multiple

unmodulated carrier signals (*i.e.*,  $f_1 + f_2 + f_3 + f_4 + f_5$ ) and processes the corresponding output of the bridge circuit to observe the impedance change of the readout coil at each carrier frequency. Since the bridge circuit is designed to be highly sensitive, the SDR can obtain the clear impedance change at each carrier frequency based on a phase spectrum. Following the phase spectrum, a peak detection algorithm [29] is applied to distinguish the typed finger by detecting the sudden phase change at each carrier frequency.

Here, we explain the working principle of our balanced bridge circuit, which is a variation of the standard Wheatstone bridge circuit [7]. This circuit has the following advantages: 1) a high signal-to-noise ratio and 2) the ease in the implementation since it requires only one reference impedance, whereas the standard bridge requires three reference impedance within 1% error. Regarding Fig. 3(c),  $V_{\text{out}}$  of the balanced bridge circuit at  $f_i$  can be written as follows using Eq. (1):

$$V_{\text{out}}(f_i) = -r_{\text{amp}} \left( \frac{V_{\text{in}}(f_i)}{Z_{\text{bridge}}} - \frac{V_{\text{in}}(f_i)}{Z_{\text{in}}(f_i)} \right) \quad (3)$$

$$= -r_{\text{amp}} \frac{Z_{\text{in}}(f_i) - Z_{\text{bridge}}}{Z_{\text{in}}(f_i)Z_{\text{bridge}}} V_{\text{in}}(f_i) \quad (4)$$

where  $V_{\text{in}}(f_i)$  denotes the input signal at  $f_i$ ,  $r_{\text{amp}}$  is the gain factor, and  $Z_{\text{bridge}}$  is the reference impedance of our balanced bridge circuit.

To enhance the sensitivity for the impedance change of the readout coil ( $\Delta Z_{\text{in}}(f_i)$ ), our balanced bridge circuit employs the *LCR*-based matching circuit for the readout coil (*i.e.*,  $Z_{\text{bridge}} \doteq Z_{\text{readout}}$ ) similar to [27]. With this,  $V_{\text{out}}$  of the bridge circuit at frequency  $f_i$  can be expressed as follows using Eq. (2) and Eq. (4):

$$V_{\text{out}}(f_i) \doteq -r_{\text{amp}} \frac{\Delta Z_{\text{in}}(f_i)}{\{Z_{\text{in}}(f_i)\}^2} V_{\text{in}}(f_i) \quad (5)$$

Using FFT, both magnitude and phase spectra of  $V_{\text{out}}$  can be obtained as follows:

$$|V_{\text{out}}(f_i)| \doteq r_{\text{amp}} \frac{\Delta Z_{\text{in}}(f_i)}{\{Z_{\text{in}}(f_i)\}^2} V_{\text{in}}(f_i) \quad (6)$$

$$\angle V_{\text{out}}(f_i) \doteq - \left( \angle \Delta Z_{\text{in}}(f_i) - \angle \{Z_{\text{in}}(f_i)\}^2 + \angle V_{\text{in}}(f_i) \right) \quad (7)$$

As will be described later,  $Z_{\text{in}}(f_i)$  is  $R : 50\Omega$ ,  $L : 4.1\mu\text{H}$ ,  $C : 33\text{pF}$  and  $|\Delta Z_{\text{in}}(f_i)|$  is approximately  $0.8\Omega$ . Based on these numerical values, the phase spectrum (Eq. (7)) is suitable in detecting the small impedance change of the readout coil since  $\Delta Z_{\text{in}}(f_i)$  can be appeared clearly through the phase change of  $V_{\text{out}}(f_i)$ . Therefore, by tracking the time-series phase of  $V_{\text{out}}(f_i)$  at each carrier frequency, the finger typing actions can be detected independently.

## IMPLEMENTATION

We describe the implementation of three hardware components of TelemetRing: the five ring-shaped sensor coils, the wristband-shaped readout coil, and the impedance measurement system, as shown in Fig. 1(a).

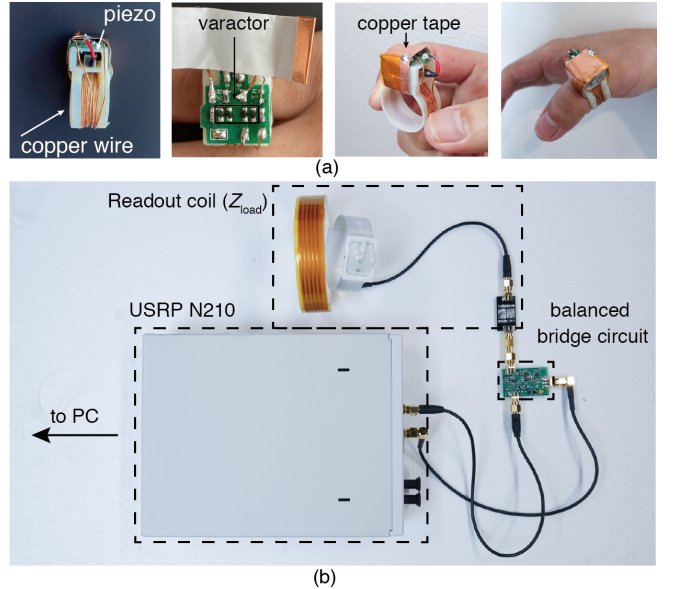


**Figure 5.** (a) Our ring-shaped sensor coil. The circuitry is covered by copper tape and connected to the ground of the sensor coil for electromagnetic shielding. (b) Our wristband-shaped readout coil and impedance measurement system.

## Ring-shaped Sensor Coil

Fig. 5(a) and Fig. 6(a) shows the prototype and the circuit model of our ring-shaped sensor, respectively. The circuit parameter can be summarized in Tab. 1. It consists of a Sekonic 110B piezoelectric accelerometer ( $C_{\text{piezo}}$ ), a Skyworks SMV series [4] varactor diode ( $C_{\text{varactor}}$ ), a tightly wound coil ( $L_{\text{sensor}}$ ), and a 3D-printed base. The coil is composed of 9-turns of  $\phi 0.5\text{ cm}$  copper wire. The base ( $16\text{ mm} \times 13\text{ mm} \times 10\text{ mm}$ ) is composed of a polypropylene-like material, which was 3D printed using a multimaterial 3D printer (Stratasys Objet260 Connex). The resonant frequency of the five sensor coils was tuned by using varactors and lumped capacitors ( $C_{\text{tuning}}$ ). The circuitry was covered by copper tape connected to the ground of the sensor coil for electromagnetic shielding. The implemented ring weighs 6 g, is 1 mm thick, and 13 mm long, and can be used at all times and on a daily basis. Moreover, the measured coupling coefficient between the five sensor coils and the wristband coil were 0.006 (#1), 0.005 (#2), 0.005 (#3), 0.005 (#4), and 0.005 (#5) from thumb to little finger;  $\|\Delta Z_{\text{in}}(f_i)\|$  was about  $0.8\Omega$ .

Herein, we explain how much capacitance (*i.e.*, impedance) of the sensor coil changes by typing. Since the shock wave propagating on the finger is reported to be  $4\text{G} \sim 8\text{G}$  and under  $100\text{ Hz}$  [11], the circuit of Fig. 6(a) can be simplified as Fig. 6(b) at such a very low frequency. With this, the bias voltage induced by typing ( $V_{\text{typing}}$ ) can be calculated as follows based on the principle of charge conservation:

$$V_{\text{typing}} \doteq \frac{Q}{C_{\text{piezo}}} \quad (C_{\text{piezo}} \gg 4 \times C_{\text{varactor}} + 2 \times C_{\text{tuning}}) \quad (8)$$

where  $Q$  is the electric charge caused by typing, whereas  $C_{\text{piezo}}$ ,  $C_{\text{varactor}}$ , and  $C_{\text{tuning}}$  are the capacitance of the piezo, varactor, and capacitor for tuning. The measured  $V_{\text{typing}}$  when

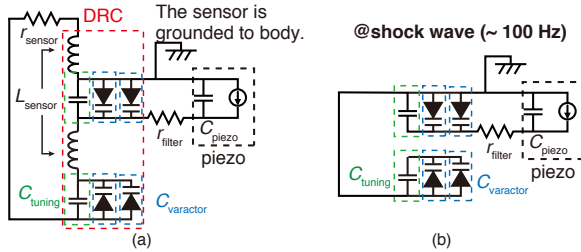


Figure 6. (a) Circuit diagram of our ring-shaped sensor coil. The simplified circuit diagram (b) at the frequency of the shock wave.

\$L_{\text{sensor}}	\$r_{\text{sensor}}	\$r_{\text{filter}}	\$C_{\text{varactor}}	\$C_{\text{piezo}}	\$C_{\text{tuning}}
\$2.2 \mu\text{H} \sim 2.5 \mu\text{H}\$	\$2.0 \Omega\$	\$100 \text{k}\Omega\$	\$50 \text{ pF} \sim 65 \text{ pF}\$	\$1.5 \text{ nF}\$	\$\sim 5 \text{ pF}\$

Table 1. Circuit parameter used in Fig. 6(a).

typing on the soft knee was approximately 100 mV, which contributes to lowering the capacitance of each varactor [4] approximately 4 pF. The total capacitance (\$C\_{\text{sensor}}\$) of our sensor coil can be approximated as follows:

$$C_{\text{sensor}} = C_{\text{varactor}}(V_{\text{typing}}) + \frac{C_{\text{tuning}}}{2} \quad (9)$$

Note that the piezo can be neglected at the carrier signal since \$r\_{\text{filter}}\$ is very high (100 k\$\Omega\$). Based on Eq. 9 and the measured \$V\_{\text{typing}}\$, it can be estimated that the capacitance of the sensor coil is lowered by approximately 1 pF (+j3\$\Omega\$) by typing.

### Wristband-shaped Readout Coil

As shown in Fig. 5(b), our readout coil is implemented on flexible PCBs (thickness: 0.1 mm, the number of turns: 5, diameter: 9 cm, line width: 1 mm, spacing: 1 mm), whereas the wristband is 3D-printed. The more number of turns increases the inductance, the wider the wristband becomes; this might impair the wearability of our wristband. For DRC, 10 capacitors (330 pF) were soldered on the flexible PCBs and the inductance was 4.1 \$\mu\$H. To decide the value of the capacitor used in DRC, first, we measured the inductance value of the readout coil at the lower frequency (*i.e.*, 1 MHz), at which the readout coil is not affected by wavelength. Based on this value (*i.e.*, 4.1 \$\mu\$H), we calculated the capacitance value. Note that the impedance of our readout coil does not almost change whether with hand or without hand because DRC lowers the electric energy, as described in SYSTEM DESIGN section. Furthermore, 49 \$\Omega\$ chip resistor was added to the readout coil in series, to satisfy \$Z\_{\text{bridge}} \approx Z\_{\text{readout}}\$.

The resonant frequency of our readout coil was set to 13.56 MHz, which is one of the ISM bands. Basically, the higher frequency of ISM band (*i.e.*, 27.12 MHz and 40.68 MHz) enables to increase the sensitivity (*i.e.*, \$\Delta Z\_{\text{in}}\$). However, we confirmed that our bridge circuit cannot work properly because the operational amplifier used in the circuit oscillated at such a high frequency. Thus, 13.56 MHz was chosen as the resonant frequency of our readout coil. Also, the resonant frequencies of our five sensor coils were tuned near 13.56 MHz. To avoid the inductive interference between the adjacent sensor coils, the five frequencies were determined by using LTspice circuit simulation [1].

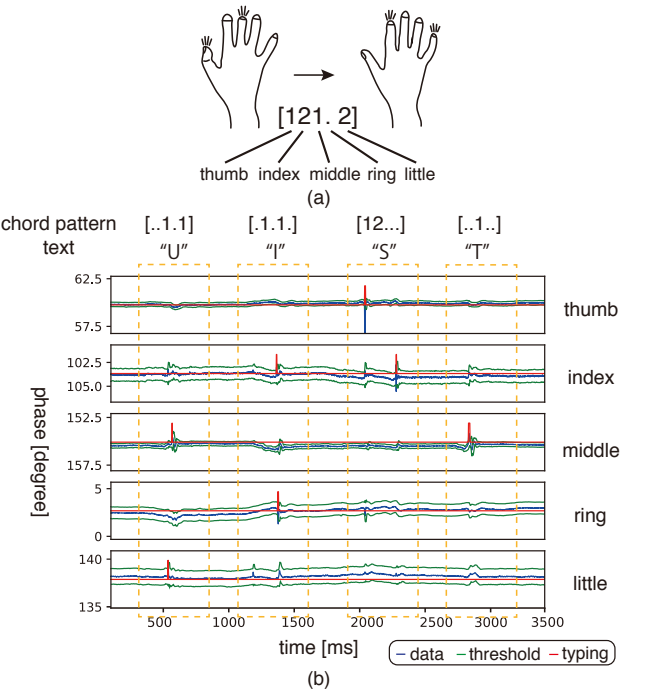


Figure 7. (a) Orderly Typing Chord Input. Chord pattern is [Thumb, Index, Middle, Ring, and Little], and the number is typing order ([.]: no type). (b) Example of typing detection when UIST was input.

### Impedance Measurement System

As shown in Fig. 5(b), our impedance measurement system is comprised of an SDR (USRP N210 [2]) and the balanced bridge circuit. The bridge circuit is implemented by OPA656 [3] (a very wideband operational amplifier, gain bandwidth product: 500 MHz) (See Fig. 3(c)). The amplifier gain \$r\_{\text{amp}}\$ is set to 100 \$\Omega\$ considering the gain bandwidth product of the OPA656. \$Z\_{\text{bridge}}\$ (\$L\_{\text{bridge}}: 4.1 \mu\text{H}\$, \$C\_{\text{bridge}}: 33 \text{ pF}\$, \$r\_{\text{bridge}}: 50 \Omega\$) is implemented using a \$4.1 \mu\text{H} + 20 \Omega\$ chip inductor, a 33 pF capacitor, and a 30 \$\Omega\$ resistor connected in series. In total, the maximum impedance error between \$Z\_{\text{bridge}}\$ and \$Z\_{\text{in}}\$ is below 5%. The power consumption of the USRP N210 and the balance bridge circuit is 7.8 W (= 6.0 V \$\times\$ 1.3 A) and 0.5 W (= 10.0 V \$\times\$ 0.05 A), respectively. While the current impedance measurement system employs the bulky and power-hungry USRP N210, we will implement a portable, low-powered, and stand-alone impedance measurement system in the future work.

### EVALUATION

This section describes the series of user studies for evaluating the typing recognition rate of TelemetRing. Note that we conducted the user studies with only one participant (*i.e.*, first author) owing to activity limitations associated with COVID-19. It is assumed that the typing recognition rate is mainly affected by 1) interference between multiple inductive channels (*e.g.*, the impedance change of the sensor coil causes the impedance change of the adjacent sensor coils and the impedance measurement system wrongly recognizes the typing of the adjacent fingers) and 2) the crosstalk caused by

typing other fingers (*e.g.*, the shock wave caused by the typing of users' middle finger propagates to the rings worn on other fingers [10]). To observe the effect of the above two factors, we conducted two experiments. In these experiments, the ground of the impedance measurement system is separated from the common ground using transformers; this is necessary since TelemetRing is separated from the common ground in real-world operations. Also, prior work shows that the crosstalk can be mitigated by using sharp bandpass filters (BPF) of 30Hz  $\sim$  100Hz [10]; therefore, we process the phase data via a digital BPF of 30Hz  $\sim$  100Hz.

In the first experiment, we investigated the interference between multiple rings. First, we prepared two types of ring-shaped sensor coils: sensor coil with piezo (S1) and sensor coil without piezo (S2). Then, the first author wore one S1 on the typed finger and four S2 on the other four fingers; ideally, only the channel with S1 will react to the typed finger. The first author typed 100 using the finger equipped with S1. Furthermore, the first author conducted a typing trial on both the desk and the knee; the strength of the shock wave is dependent on the softness of the typing surface (*i.e.*, hard desk: 8G, soft knee: 4G), so this data was used to adjust the thresholds of typing detection. Overall, the total trial is 1000 times (100 typing, 2 types of surfaces, and 5 fingers). Tab. 2 shows the typing recognition rate of five channels. The average recognition rate was 95.9% on both the desk and the knee, which indicates that there exists little interference between frequency channels.

In the second experiment, we examined the recognition rate of various typing chords considering both the interference between multiple inductive channels and the crosstalk caused by other fingers' typing. Similar to the previous ring-shaped keyboards [11, 10], TelemetRing supports text entry by simultaneously typing some of five fingers based on a typing chord, as shown in Fig. 7(a). To examine the recognition rate of each typing chord, all the 31 chord patterns that can be represented by one-stroke typing were tested (See the chord column in Tab. 3). The first author typed each chord 100 times on the hard desk. Note that the typing surface was only the hard desk since there is little difference between the recognition rate on the hard desk and the soft knee, as shown in Tab. 2.

Tab. 3 shows the typing recognition rate for 31 chord patterns. It is confirmed that the four chords ([11.1], [.1.11], [111.1], [11.11]) result in the very low recognition rate. This is because these typing chords are difficult to type owing to the skeleton of our hand [30]; for example, the typing using both middle and little fingers inevitably induces the typing of the ring finger. Therefore, our chord pattern that assigns the input commands (A-Z characters, numbers, etc.) to the typing chords are similar to [10] since it eliminates chord patterns that are difficult to type. With 27 chord patterns excluding the above 4 chord patterns, TelemetRing achieves the chord input with 10.3% error and enables to input text "UIST" (See Fig. 7(b)).

While TelemetRing enables to input short words (*e.g.*, *uist* or *hello*) accurately, the input of long sentences (*e.g.*, *this is a pen.*) without mistakes is difficult with 10.3% recognition

place	thumb ( $f_1$ )	index ( $f_3$ )	middle ( $f_5$ )	ring ( $f_2$ )	little ( $f_4$ )
desk	95%	95%	96%	93%	100%
knee	100%	96%	93%	94%	97%

Table 2. Recognition rate for fingers and typing surfaces.

chord [T,I,M,R,L]	desk	chord [T,I,M,R,L]	desk	chord [T,I,M,R,L]	desk
[1....]	93%	[.1.1.]	89%	[1..11]	84%
[.1..]	97%	[.1..1]	85%	[.111.]	93%
[..1..]	96%	[..11.]	96%	[.11..1]	59%
[...1.]	90%	[...1.1]	82%	[.1..11]	55%
[....1]	96%	[...11]	87%	[..111]	91%
[11...]	90%	[111..]	98%	[1111..]	91%
[1..1..]	89%	[11..1.]	78%	[111..1]	61%
[1..1..]	89%	[11..1.]	90%	[11..11]	25%
[1...1.]	93%	[1..11.]	91%	[1..111]	87%
[.11..]	91%	[.1.1.1]	88%	[.1111.]	87%
				[11111]	80%

Table 3. Recognition rate of 31 chord pattern. the number (1) of typing pattern [Thumb, Index, Middle, Ring, Little] is the typed finger and [.] means no type.

error. This error might be mainly attributed to the digital BPF, which can not completely suppress the noise caused by the variation of both the inductive coupling and the coupling with the body. The recognition rate could be improved through optimized signal processing (*e.g.*, short-time Fourier transform filter).

## LIMITATIONS AND FUTURE WORK

TelemetRing has some limitations and future work. First, the typing recognition rate is evaluated with only one person. To understand the recognition rate independent of individuals, we must conduct user studies with more than 10 participants, similar to previous ring-shaped keyboards [11, 23]. Such a evaluation will help us to set parameters that can be used by anyone regardless of gender and age. Another limitation of the current implementation is that the equipped off-the-shelf high-sensitive piezo makes the base of the current ring cumbersome. The development of small and self-powered MEMS shock sensors is a promising candidate for substituting this cumbersome sensor and will lead to a truly miniature ring.

## CONCLUSION

This paper proposed TelemetRing, a batteryless and wireless ring-shaped keyboard that supports text entry by detecting finger typing. The keyboard leverages the passive inductive telemetry to enable batteryless ring-shaped sensors. With the combination of the DRC and the balanced bridge circuit, our passive inductive telemetry can detect typing actions with a recognition accuracy of 89.7%. We envision that our passive inductive telemetry system can be applied to other wearable devices in addition to TelemetRing.

## ACKNOWLEDGMENTS

This work was supported by JST ERATO, Japan under Grant No.: JPMJER1501. We would like to thank Takashi Ikeuchi for his help of TelemetRing's implementation.

## REFERENCES

- [1] 2011. LTspice. (2011). Retrieved July 4, 2020 from <https://www.analog.com/media/en/simulation-models/spice-models/LTspiceGettingStartedGuide.pdf?modelType=spice-models>
- [2] 2012. USRP N200/N210 NETWORKED SERIES. (2012). Retrieved July 4, 2020 from [https://www.ettus.com/wp-content/uploads/2019/01/07495\\_Ettus\\_N200-210\\_DS\\_Flyer\\_HR\\_1.pdf](https://www.ettus.com/wp-content/uploads/2019/01/07495_Ettus_N200-210_DS_Flyer_HR_1.pdf)
- [3] 2015. OPA656. (2015). Retrieved July 4, 2020 from <http://www.tij.co.jp/jp/lit/ds/symlink/opa656.pdf>
- [4] 2016. SMV1255 SERIES. (2016). Retrieved July 4, 2020 from <https://www.skyworksinc.com/products/diodes/smv1255-series>
- [5] R. Bainbridge and J. A. Paradiso. 2011. Wireless Hand Gesture Capture through Wearable Passive Tag Sensing. In *2011 International Conference on Body Sensor Networks*. 200–204.
- [6] Kaikai Bao, Deyong Chen, Qiang Shi, Jian Chen, and Junbo Wang. 2013. A readout circuit for wireless passive resonant-circuit sensors. In *2013 IEEE SENSORS*. IEEE, 1–4. DOI: <http://dx.doi.org/10.1109/ICSENS.2013.6688262>
- [7] Larry K Baxter. 1997. Capacitive sensors. *Design and Applications* (1997).
- [8] Liwei Chan, Yi-Ling Chen, Chi-Hao Hsieh, Rong-Hao Liang, and Bing-Yu Chen. 2015. CyclopsRing: Enabling Whole-Hand and Context-Aware Interactions Through a Fisheye Ring. In *Proceedings of the 28th Annual ACM Symposium on User Interface Software & Technology - UIST '15*. ACM Press, New York, NY, USA, 549–556. DOI: <http://dx.doi.org/10.1145/2807442.2807450>
- [9] Ke-Yu Chen, Shwetak N. Patel, and Sean Keller. 2016. Finexus: Tracking Precise Motions of Multiple Fingertips Using Magnetic Sensing. In *Proceedings of the 2016 CHI Conference on Human Factors in Computing Systems*. ACM, New York, NY, USA, 1504–1514. DOI: <http://dx.doi.org/10.1145/2858036.2858125>
- [10] Masaaki Fukumoto and Yasuhito Suenaga. 1994. "FingeRing": A full-time wearable interface. *Conference on Human Factors in Computing Systems - Proceedings* (1994), 81–82. DOI: <http://dx.doi.org/10.1145/259963.260056>
- [11] Masaaki Fukumoto and Yoshinobu Tonomura. 1997. "Body coupled FingerRing": Wireless Wearable Keyboard. In *Proceedings of the SIGCHI conference on Human factors in computing systems - CHI '97*. ACM Press, New York, NY, USA, 147–154. DOI: <http://dx.doi.org/10.1145/258549.258636>
- [12] Tovi Grossman, Xiang Anthony Chen, and George Fitzmaurice. 2015. Typing on Glasses: Adapting Text Entry to Smart Eyewear. In *Proceedings of the 17th International Conference on Human-Computer Interaction with Mobile Devices and Services - MobileHCI '15*. ACM Press, New York, NY, USA, 144–152. DOI: <http://dx.doi.org/10.1145/2785830.2785867>
- [13] Aakar Gupta, Cheng Ji, Hui-Shyong Yeo, Aaron Quigley, and Daniel Vogel. 2019. RotoSwype: Word-Gesture Typing Using a Ring. In *Proceedings of the 2019 CHI Conference on Human Factors in Computing Systems (CHI '19)*. Association for Computing Machinery, New York, NY, USA, 1–12. DOI: <http://dx.doi.org/10.1145/3290605.3300244>
- [14] Chris Harrison, Desney Tan, and Dan Morris. 2010. Skinput: Appropriating the Body as an Input Surface. In *Proceedings of the 28th international conference on Human factors in computing systems - CHI '10*. ACM Press, New York, NY, USA, 453. DOI: <http://dx.doi.org/10.1145/1753326.1753394>
- [15] Kai-yuh Hsiao. 2001. *Fast Multi-Axis Tracking of Magnetically-Resonant Passive Tags: Methods and Applications*. Ph.D. Dissertation. Massachusetts Institute of Technology.
- [16] Jiawei Huang, Tsuyoshi Mori, Kazuki Takashima, Shuichiro Hashi, and Yoshifumi Kitamura. 2015. IM6D: Magnetic Tracking System with 6-DOF Passive Markers for Dexterous 3D Interaction and Motion. *ACM Trans. Graph.* 34, 6, Article 217 (Oct. 2015), 10 pages. DOI: <http://dx.doi.org/10.1145/2816795.2818135>
- [17] Qing An Huang, Lei Dong, and Li Feng Wang. 2016. LC Passive Wireless Sensors Toward a Wireless Sensing Platform: Status, Prospects, and Challenges. *Journal of Microelectromechanical Systems* 25, 5 (2016), 822–841. DOI: <http://dx.doi.org/10.1109/JMEMS.2016.2602298>
- [18] Yasha Iravantchi, Mayank Goel, and Chris Harrison. 2019. BeamBand: Hand Gesture Sensing with Ultrasonic Beamforming. In *Proceedings of the 2019 CHI Conference on Human Factors in Computing Systems - CHI '19*. ACM Press, New York, NY, USA, 1–10. DOI: <http://dx.doi.org/10.1145/3290605.3300245>
- [19] David Kim, Otmar Hilliges, Shahram Izadi, Alex Butler, Jiawen Chen, Iason Oikonomidis, and Patrick Olivier. 2012. Digits: Freehand 3D interactions anywhere using a wrist-worn gloveless sensor. *UIST'12 - Proceedings of the 25th Annual ACM Symposium on User Interface Software and Technology* (2012), 167–176.
- [20] André Kurs, Aristeidis Karalis, Robert Moffatt, J. D. Joannopoulos, Peter Fisher, and M. Soljacic. 2007. Wireless Power Transfer via Strongly Coupled Magnetic Resonances. *Science* 317, 5834 (2007), 83–86. DOI: <http://dx.doi.org/10.1126/science.1143254>
- [21] Gierad Laput, Robert Xiao, and Chris Harrison. 2016. ViBand: High-Fidelity Bio-Acoustic Sensing Using Commodity Smartwatch Accelerometers. In *Proceedings of the 29th Annual Symposium on User Interface Software and Technology - UIST '16*. ACM Press, New York, NY, USA, 321–333. DOI: <http://dx.doi.org/10.1145/2984511.2984582>

- [22] Kent Lyons, Thad Starner, Daniel Plaisted, James Fusia, Amanda Lyons, Aaron Drew, and E. W. Looney. 2004. Twiddler Typing: One-Handed Chording Text Entry for Mobile Phones. In *Proceedings of the SIGCHI Conference on Human Factors in Computing Systems (CHI '04)*. Association for Computing Machinery, New York, NY, USA, 671–678. DOI: <http://dx.doi.org/10.1145/985692.985777>
- [23] Damien Masson, Alix Goguey, Sylvain Malacria, and Géry Casiez. 2017. WhichFingers: Identifying Fingers on Touch Surfaces and Keyboards using Vibration Sensors. In *Proceedings of the 30th Annual ACM Symposium on User Interface Software and Technology - UIST '17*. ACM Press, New York, NY, USA, 41–48. DOI: <http://dx.doi.org/10.1145/3126594.3126619>
- [24] R. A. Moffatt, T. Howarth, C. Gafner, J. J. Yen, F. Chen, and J. Yu. 2019. A Distributed, Phase-locked, Class-E, RF Generator with Automatic Zero-Voltage Switching. In *2019 IEEE Wireless Power Transfer Conference (WPTC)*. 390–394.
- [25] Yoshiaki Narusue and Yoshihiro Kawahara. 2017. Distributed reactance compensation for printed spiral coils in wireless power transfer. In *2017 IEEE Wireless Power Transfer Conference (WPTC)*. IEEE, 1–4. DOI: <http://dx.doi.org/10.1109/WPT.2017.7953904>
- [26] International Commission on Non-Ionizing Radiation Protection and others. 2009. ICNIRP statement on the guidelines for limiting exposure to time-varying electric, magnetic, and electromagnetic fields (up to 300 GHz). *Health physics* 97, 3 (2009), 257–258.
- [27] Joseph A. Paradiso, Laurel S. Pardue, Kai-Yuh Hsiao, and Ari Y. Benbasat. 2003. Electromagnetic Tagging for Electronic Music Interfaces. *Journal of New Music Research* 32, 4 (2003), 395–409. DOI: <http://dx.doi.org/10.1076/jnmr.32.4.395.18858>
- [28] Farshid Salemi Parizi, Eric Whitmire, and Shwetak Patel. 2019. AuraRing: Precise Electromagnetic Finger Tracking. *Proceedings of the ACM on Interactive, Mobile, Wearable and Ubiquitous Technologies* 3, 4 (12 2019), 1–28. DOI: <http://dx.doi.org/10.1145/3369831>
- [29] J. Paul. 2014. Smoothed Z Score Algorithm. (2014). Retrieved March 1, 2020 from <https://stackoverflow.com/questions/22583391>
- [30] Reinhard Putz and Reinhard Pabst. 2006. *Sobotta-Atlas of Human Anatomy: Head, Neck, Upper Limb, Thorax, Abdomen, Pelvis, Lower Limb; Two-volume set*.
- [31] Anil Kumar RamRakhiani, Shahriar Mirabbasi, and Mu Chiao. 2011. Design and Optimization of Resonance-Based Efficient Wireless Power Delivery Systems for Biomedical Implants. *IEEE Transactions on Biomedical Circuits and Systems* 5, 1 (2 2011), 48–63. DOI: <http://dx.doi.org/10.1109/TBCAS.2010.2072782>
- [32] J. Rekimoto. 2001. GestureWrist and GesturePad: unobtrusive wearable interaction devices. In *Proceedings Fifth International Symposium on Wearable Computers*. 21–27.
- [33] T. Scott Saponas, Desney S. Tan, Dan Morris, Ravin Balakrishnan, Jim Turner, and James A. Landay. 2009. Enabling always-available input with muscle-computer interfaces. *UIST 2009 - Proceedings of the 22nd Annual ACM Symposium on User Interface Software and Technology* (2009), 167–176. DOI: <http://dx.doi.org/10.1145/1622176.1622208>
- [34] Andrew Vardy, John Robinson, and Li-Te Cheng. 1999. The WristCam as input device. In *Digest of Papers. Third International Symposium on Wearable Computers*. IEEE Comput. Soc, 199–202. DOI: <http://dx.doi.org/10.1109/ISWC.1999.806928>
- [35] Zheer Xu, Pui Chung Wong, Jun Gong, Te-Yen Wu, Aditya Shekhar Nittala, Xiaojun Bi, Jürgen Steimle, Hongbo Fu, Kening Zhu, and Xing-Dong Yang. 2019. TipText: Eyes-Free Text Entry on a Fingertip Keyboard. In *Proceedings of the 32nd Annual ACM Symposium on User Interface Software and Technology*. ACM, New York, NY, USA, 883–899. DOI: <http://dx.doi.org/10.1145/3332165.3347865>
- [36] Yang Zhang, Junhan Zhou, Gierad Laput, and Chris Harrison. 2016. SkinTrack: Using the Body as an Electrical Waveguide for Continuous Finger Tracking on the Skin. In *Proceedings of the 2016 CHI Conference on Human Factors in Computing Systems - CHI '16*. ACM Press, New York, NY, USA, 1491–1503. DOI: <http://dx.doi.org/10.1145/2858036.2858082>